journal

J. Am. Ceram. Soc., 1–7 (2015)
DOI: 10.1111/jace.13766

Melter Feed Reactions at $T \leq 700°C$ for Nuclear Waste Vitrification

Kai Xu,† Pavel Hrma, Jarrett Rice, Brian J. Riley, Michael J. Schweiger, and Jarrod V. Crum

Pacific Northwest National Laboratory, Richland, Washington 99352

To understand feed-to-glass conversion for the vitrification of nuclear waste, we investigated batch reactions and phase transitions in a simulated nuclear waste glass melter feed heated at 5 K/min up to 700°C using optical microscopy, scanning electron microscopy with energy-dispersive X-ray spectroscopy, and X-ray diffraction. To determine the content and composition of leachable phases, we performed leaching tests; the leachates were analyzed by inductively coupled plasma atomic emission spectroscopy. By 400°C, gibbsite and sodium borates lost water and converted to amorphous phase, whereas other metallic hydroxides dehydrated to oxides. Between 400°C and 700°C, carbonates decomposed before 500°C; amorphous aluminum oxide and calcium oxide reacted with the sodium borate and formed the more durable amorphous borate phase along with intermediate crystalline products; above 500°C, quartz began to dissolve, and hematite started to convert to trevorite.

I. Introduction

In a typical joule-heated nuclear waste glass melter at Hanford, the feed—a slurry mixture of waste with glass-forming and glass-modifying additives—is charged on the top of the cold cap (i.e., in commercial glass parlance, the batch blanket).[1] The cold cap covers 90%–100% of the melt surface.[2] The feed is converted to molten glass as it moves down through the cold cap from the top, where the temperature can be as low as 100°C (if covered by slurry), to the bottom, where the temperature (typically ~1100°C) depends on the intensity of melt stirring.[3–5] Unlike commercial glass batches, the nuclear waste feed typically contains approximately 50 mass% water and more than 20 chemical components including water-soluble salts, amorphous gels, and crystalline minerals.[6–8] Thus, multiple batch reactions and phase transitions occur during the passage of the feed through the cold cap. This feed-to-glass conversion usually comprises five steps: (i) evaporation and release of water, (ii) melting and decomposition of oxy-ionic salts and borates, (iii) formation of intermediate phases, (iv) dissolution of quartz, and (v) expansion and collapse of foam. Understanding batch reactions and phase transitions within the cold-cap temperature range is supportive for modeling efforts and the melter feed formulation to maximize the waste glass processing rate.[9,10]

Batch reactions of soda-silicate or soda-lime-silicate glasses have been extensively investigated using various techniques, including Raman spectroscopy,[11] thermal analysis,[12–14] and magic-angle spinning nuclear magnetic resonance spectroscopy,[15] as well as *in situ* measurements including optical microscopy,[16] X-ray diffraction (XRD),[17–19] and X-ray tomography.[20] Early batch melting studies were reviewed by Hrma et al.[21,22] For high-level waste glass melting, understanding the reaction kinetics and glass-batch formulation has been of interest for increasing the processing rate.[22–25] For example, using gibbsite instead of corundum as an alumina source produced substantially less foaming, thus increasing the melting rate.[25] The structure and reactions of simulated waste feeds in the cold cap were nondestructively investigated for the size and spatial distribution of bubbles and insoluble residues by X-ray imaging techniques.[26,27] The kinetics of the feed-to-glass conversion was modeled as a series of independent multiple overlapping *n*th-order reactions, the parameters of which were obtained by fitting model equations to thermal analysis data.[28,29] More recent work employed evolved gas analysis (EGA) via quantitative gas chromatography-mass spectrometry to identify evolution kinetics of each gas.[30]

In spite of the extensive studies listed above, our knowledge of the transition of waste glass melter feed to molten glass is still incomplete. Especially lacking is information about the formation of liquid phases. The molten salt phase appears early in the melting process due to low-temperature eutectics. The first borate glass formation probably appears parallel with the molten salt phase. Whereas the molten salt phase shrinks and simplifies in composition, turning from the initial predominantly NO_3^-–NO_2^-–CO_3^{2-}–SO_4^{2-} melt to the residual SO_4^{2-} melt, the borate melt dissolves more and more feed components, eventually turning into the final borosilicate composition.

These processes can be observed only indirectly. By analyzing the content of crystalline phases with XRD, we can make inferences regarding the amorphous residue in the quenched samples. Leaching the samples in cold and hot water and analyzing the leachates allows us to assess the contents and compositions of the salt phase and the early glass-forming (borate) phase. This way we can obtain more detailed information about the batch reactions and phase transitions.

The knowledge gained will enhance our understanding of the conversion of melter feed to molten glass, and also elucidate the behavior of volatile components, such as T_c and I.[31] In this study, we focused on batch reactions that occurred before the gas evolution was complete[28,30] and the volume of glass feed significantly shrank,[24,25] in particular during heating at a constant rate to 700°C. Above this temperature, significant changes occur with the formation of a connected melt, foaming and the dissolution of quartz.

II. Experimental Procedure

(1) Feed Preparation and Heat Treatment

The melter feed used in this study (Table I) was initially designed for the Hanford Waste Treatment and Immobilization Plant for vitrification of a high-level radioactive waste with a high-alumina content.[32] The simulated feed was prepared as slurry, as described in a previous study,[33] mixed and dried on a hot plate, and then heated at 105°C overnight in an oven. Silica was added as crushed quartz with maximum particle size of 75 μm. Dry feed samples of ~10 g were heated at the rate of 5 K/min from room temperature to the target temperature range from 200°C to 700°C in porcelain crucibles and then quickly removed from the furnace to quench in air.

E. Vance—contributing editor

Manuscript No. 36331. Received January 28, 2015; approved June 15, 2015.
†Author to whom correspondence should be addressed. e-mail: kai.xu@pnnl.gov

(2) Characterization of Heat-Treated Feed Samples

Two representative samples heat treated to 400°C and 600°C were examined with an optical microscope (SZH 10; Olympus, Center Valley, PA) and a scanning electron microscope (SEM) (JSM-7001F; JEOL USA, Inc., Peabody, MA) for morphology and crystalline phase analyses. Energy-dispersive spectroscopy was performed with an EDAX Si-drift energy-dispersive X-ray spectroscope (EDS) (Apollo XL; AMETEK, Berwyn, PA) for elemental dot mapping to determine the compositions of the various phases. The heat-treated samples, which remained in the form of powder, were cast in an epoxy resin and polished in an oil-based diamond suspension to prevent dissolution of water-soluble species before analysis.

Samples were heated up to 700°C in 100°C intervals. Crystalline phase identification and quantification in the heat-treated samples were accomplished by XRD analysis with a Bruker D8 Advance diffractometer (Bruker AXS Inc., Madison, WI) equipped with a CuK_α target at a power of 40 kV and 40 mA. Representative portions of heat-treated samples were mixed with 5 mass% CaF_2 as an internal standard and crushed in a tungsten carbide mill. Samples were scanned from 5° to 80° 2θ at a step size of 0.015° 2θ with a dwell time of 1.5 s per step. Crystalline phases were identified with Bruker AXS DIFFRAC^{plus} EVA software and quantitative fractions of the crystalline phases were determined by fitting whole patterns with TOPAS 4.2 software (Bruker AXS Inc.).

(3) Leaching of Heat-Treated Feed Samples

To determine the content and composition of leachable phases, an independent heat-treatment series was performed. Leaching tests were conducted on three representative samples heat treated to temperatures of 105°C (as-prepared), 350°C (almost no hydrated water remained), and 550°C (intermediate crystalline phases formed). Heat-treated samples were lightly crushed using an agate mortar and pestle to refine the large clumps. Then 5 g (±0.0001 g) of each sample and 100 mL deionized water (DIW) from a graduated cylinder were added to a 250-mL Pyrex beaker at room temperature. An aliquot of 10 ml solution was taken out using a 10-mL syringe with a 0.45-μm filter for elemental analysis with inductively coupled plasma atomic emission spectroscopy after 10 and 70 min had elapsed at room temperature. The beaker was replenished with 10 mL of fresh DIW after each 10 ml aliquot was removed to maintain a constant volume in the beaker.

Beakers were then covered with lids and transferred to an 80°C water bath. This higher temperature was used to dissolve the more durable borate phases. Aliquots of 10 mL were taken out after exposure for 60 min (and also after 24 h for the 550°C sample) for elemental analysis. Because of the experimental uncertainty, the leaching test shows the dissolution trends of leachable phases as functions of heat-treatment temperature, but provides only approximate values of the content of those phases.

Table I. Batch Composition (g) to Make 1 kg of Glass and Target Glass Composition

Batch composition	g/kg	Glass composition	Mass%	Mol%
SiO_2	305.05	SiO_2	30.50	35.05
$Al(OH)_3$	367.49	Al_2O_3	24.00	16.25
H_3BO_3	269.83	B_2O_3	15.21	15.09
Li_2CO_3	88.30	Li_2O	3.57	8.25
CaO	60.79	CaO	6.09	7.50
$Fe(OH)_3$	73.82	Fe_2O_3	5.91	2.56
$Fe(H_2PO_2)_3$	12.42	Na_2O	9.59	10.68
NaOH	99.41	K_2O	0.14	0.10
NaF	14.78	MgO	0.12	0.21
Na_2CrO_4	11.13	ZrO_2	0.39	0.22
Na_2SO_4	3.55	ZnO	0.08	0.07
$NaNO_2$	3.37	Bi_2O_3	1.14	0.17
$Na_2C_2O_4$	1.26	NiO	0.40	0.37
KNO_3	3.04	PbO	0.41	0.13
$Mg(OH)_2$	1.69	Cr_2O_3	0.52	0.24
$Zr(OH)_4{\cdot}0.65H_2O$	5.49	P_2O_5	1.05	0.51
$Zn(NO_3)_2{\cdot}4H_2O$	2.67	SO_3	0.20	0.17
$Bi(OH)_3$	12.80	F	0.67	2.44
$NiCO_3$	6.36			
$Pb(NO_3)_2$	6.08			
Total	1349.33	Total	100.00	100.00

(4) Data Processing

When melter feed is subjected to heat treatment at continuously increasing temperature, it gradually loses mass as gases evolve. We express the content of chemical and crystalline constituents in samples, originally recorded with respect to the sample mass, as the mass fraction related either to the initial dry feed or to the final glass as in the following formula:

$$x_c = y_c \frac{m_s}{m_g} \tag{1}$$

where x_c is the cth crystalline phase mass fraction with respect to glass, y_c is the cth phase mass fraction in the sample (as determined with XRD), m_s is the sample mass, and m_g is the final glass mass.

Unlike glass produced in large-scale melters, the laboratory samples have a large surface-to-volume ratio and thus are subjected to volatilization, especially at temperatures higher than 800°C. Here, we took for m_g in a sample heated to ~700°C, the temperature at which the gas-liberating reactions had virtually ceased and volatilization and oxygen release from redox reactions were still imperceptible.[28,30]

As shown in Table I, the feed-to-glass mass ratio, f_s, based on the stoichiometry of the batched chemicals, is 1.349. However, because of the loss of bonded water and absorption of CO_2 from the air during slurry preparation and subsequent drying, the dry feed-to-glass mass ratio, f_a, is different from f_s. Because the mass-loss fraction of the present feed heated to 700°C in the crucible test is 0.2158, $f_a = 1.275$ and $m_g = m_f/f_a$, where m_f is the dry sample mass. Thus, Eq. (1) can be alternatively expressed in terms of the initial sample mass as

$$x_c = y_c f_a \frac{m_s}{m_f} \tag{2}$$

where m_s/m_f is the mass fraction remaining after heating.

As described in Section II(3), solution samples were repeatedly removed for analysis and replenished with aliquots of water. After the kth replenishment, the total ith element mass dissolved (m_{dik}) was

$$m_{dik} = Vc_{ik} + V_S \sum_{j=1}^{k-1} c_{ij} \tag{3}$$

where V is the solution volume (100 mL), V_s is the solution sample volume (10 mL), and c_{ij} is the ith element concentration (mass per volume) in the solution just before kth replenishment; the subscript d denotes "dissolved."

The fraction of the ith element dissolved per element in glass (i.e., element dissolved per element total) is $z_i = m_{di}/m_{gi}$, where m_{di} is the ith element mass dissolved. The mass of the ith element in the glass is $m_{gi} = m_g g_i$, where g_i is the ith element mass fraction in glass. By Eq. (3)

$$z_{ik} = \frac{V}{m_g g_i}\left(c_{ik} + v_s \sum_{j=1}^{k-1} c_{ij}\right) \quad (4)$$

where $v_s = V_s/V = 0.1$.

For 5 g of as-prepared feed sample, the corresponding mass of glass, $m_{g,105} = m_s/f_a = 5/1.275 = 3.92$ g. According to the mass-loss test, the 350°C and 550°C treated feed-to-glass mass ratios are $f_{a,350} = 1.166$ and $f_{a,550} = 1.049$. Thus, corresponding masses of glasses $m_{g,350}$ and $m_{g,550}$ were 4.29 and 4.77 g, respectively.

III. Results

Samples heated to ≤600°C were soft and crumbled easily, whereas the sample heated to 700°C became relatively firm and its volume visually shrank. Figures 1(a)–(c) display optical and SEM micrographs and an elemental EDS phase map of a feed sample heated to 400°C. The images show isolated grains and agglomerated clusters that formed during initial drying. Ten regions, shown boxed in Fig. 1(b), were investigated with EDS. The regions show grains and agglomerates containing Si (1, 2), Fe (3, 4, 5), Bi (6), Zr (7), Na (8), Al, Na, and Ca (9), and Ca with Na (10), Fig. 1(c). Similar optical and SEM-EDS analyses were performed for a sample heated to 600°C (Fig. 2). As shown in Figs. 2(b) and (c), grains of quartz (1) remained virtually unchanged, with the particles retaining sharp edges. Regions rich in Zr (2), Fe (3, 4), and Bi (6) have not been dispersed yet. However, Al clustered with Na and, to a lesser extent, Ca became dispersed throughout the feed as fine particles smaller than 1 μm.

Figures 3(a) and (b) plot the changes of major and minor phases in feed samples determined by XRD in response to the temperature to which the samples were heated. As shown in Fig. 3(a), quartz (SiO_2) was present in all samples at consistent levels until 500°C and then showed a tendency to decrease. The fraction of gibbsite [$Al(OH)_3$] decreased dramatically between 200°C and 300°C, dropping to zero by 400°C. A small fraction of boehmite (AlOOH) that had occurred in the initial dry feed increased as the temperature reached 300°C and remained at approximately the same level during heating to 600°C, but finally disappeared by 700°C. The amorphous phase gradually increased as the temperature increased to 500°C and then decreased. The intermediate borate crystalline phase, $Ca_{0.5}NaAl_2B_2O_7$, appeared at 500°C and continued to increase as the temperature reached 700°C (the possibility cannot be ruled out that the content of $Ca_{0.5}NaAl_2B_2O_7$ phase increased during sample quenching). Of minor crystalline phases [Fig. 3(b)], hematite (Fe_2O_3) and trevorite ($NiFe_2O_4$) had already formed in the initial dry feed. While hematite somewhat increased as the temperature increased to 400°C and started to decrease after 500°C, trevorite remained at a nearly constant fraction until 500°C and then showed a tendency to increase. Sodalite-nosean [$Na_8(AlSiO_4)_6(SO_4)$] began to emerge at 600°C. Calcite ($CaCO_3$), zabuyelite (Li_2CO_3), and thenardite (Na_2SO_4) disappeared by 500°C. Crystallization of other salts was not observed by XRD. With the possible exception mentioned above, it is unlikely that crystallinity of the samples was affected by quenching.

Additional information about the development of water-soluble and early glass-forming phases was gained by analyzing the leachates. Table II lists the fractions of elements (Na, B, Li, S, and Al) dissolved, calculated with Eq. (4), from heat-treated feeds at each leaching step. Figure 4(a) compares dissolved fractions of Na and B at each leaching step as functions of heat-treatment temperature, whereas Figs. 4(b) and (c) plot dissolved fractions of Li and Al, respectively, versus heat-treatment temperature. The dissolved fractions of Na and B are similar [Fig. 4(a)] and higher than those of Li [Fig. 4(b)]. Whereas dissolved fractions of Na, B, and Li (and also S, Table II) at each leaching step decreased as the heat-treatment temperature increased, the dissolved fractions of Al increased with the heat-treatment temperature [Fig. 4(c)].

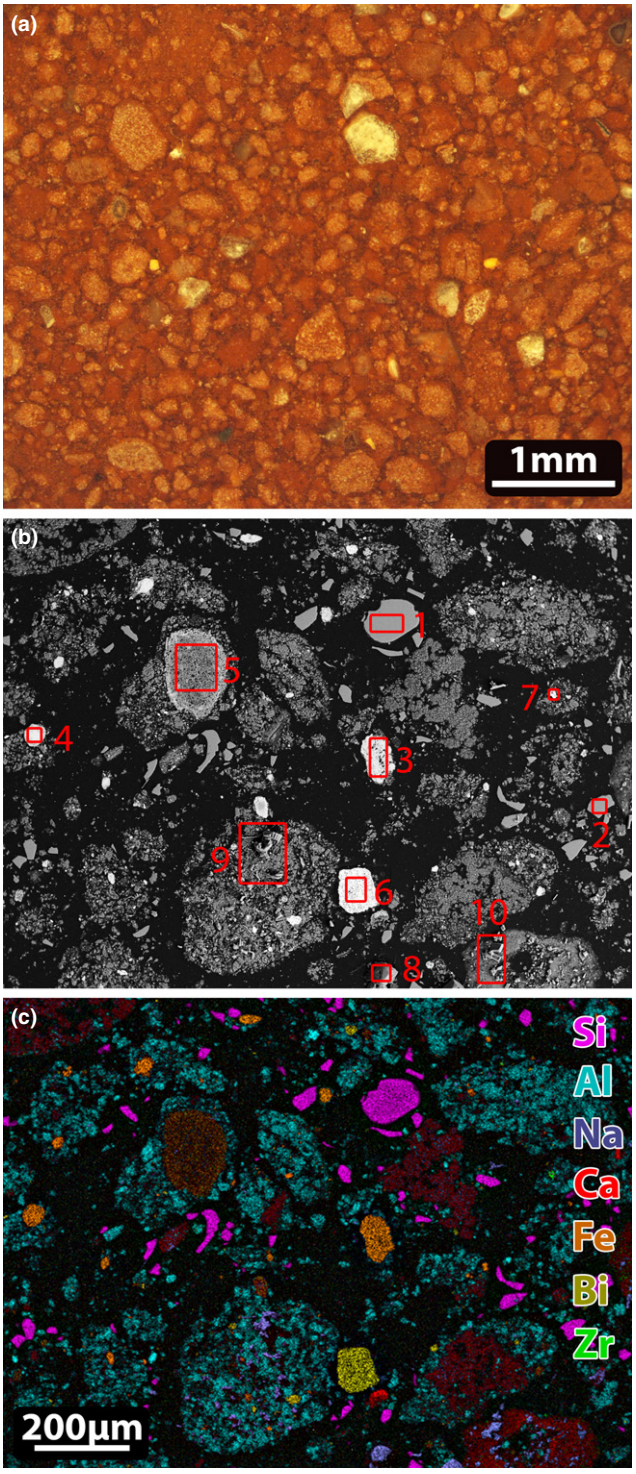

Fig. 1. (a) Optical and (b) SEM micrographs, and (c) EDS elemental mapping of feed sample heated to 400°C. Areas marked in (b) are element-rich regions of Si (1, 2), Fe (3, 4, 5), Bi (6), Zr (7), Na (8), Al, Na and Ca (9), and Ca and Na (10). Note that the looser aggregate 5 appears darker than the denser ones (3 and 4).

Elements that dissolved in DIW at room temperature are indicative of the presence of water-soluble salts in the samples. The salts dissolved rapidly: only 3% more Na and B dissolved from dry feed in 70 min than in 10 min, and all S dissolved in only 10 min (Table II). Over 90% of Na and B and only ~80% of Li dissolved from the dry feed, whereas less than 1% of Al was leached. Hot-water leaching of dry

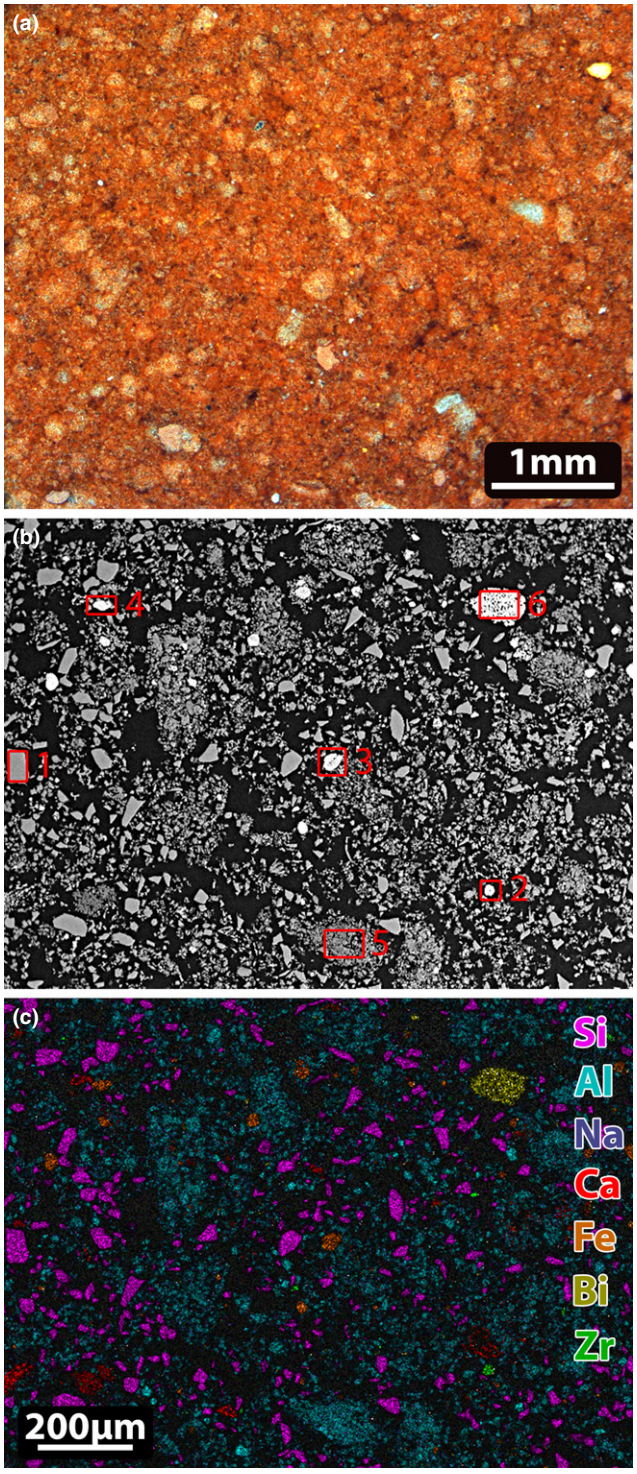

Fig. 2. (a) Optical, (b) SEM micrographs, and (c) EDS elemental mapping of feed sample heated to 600°C. Areas marked in (b) are element-rich regions of Si (1), Zr (2), Fe (3, 4), Al and Na (5), and Bi (6).

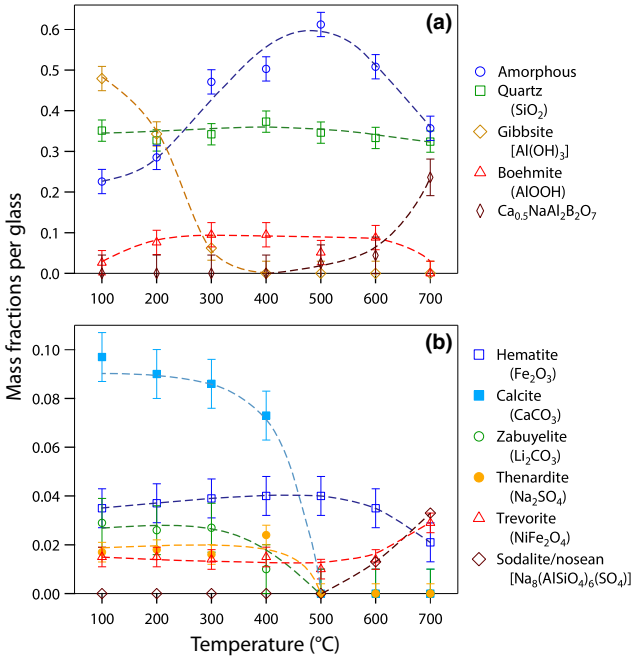

Fig. 3. Mass fractions of (a) major and (b) minor phases in feed samples with respect to glass versus heat-treatment temperatures. Dashed lines were added as guides to the eyes. The error bars indicate the standard deviations based on the XRD tests for the two identical samples.

feed dissolved only ~4% additional Na and B. These results indicate that Na and B remained in the form of soluble phases after the slurry feed was dried, even though not all Na and B were dissolved either in room-temperature water or in hot water.

The increase in leaching time from 10 to 70 min at room temperature substantially increased the release of Na and B from samples heat treated to 350°C and 550°C. The dissolved fractions of Na and B increased by ~36% for 1 h of additional leaching (beyond the first 10 min) at 350°C and by ~82% at 550°C (Table II). These relatively low leaching rates rule out the dissolution of inorganic salts, which mostly dissolved in the first 10 min, and indicate the presence of low-durability borate amorphous phases in the samples. This assertion is supported by data from 60-min leaching in hot (80°C) water: the dissolved fraction of alkali and B increased by ~20% at 350°C and by ~50% (~26% of Li) at 550°C (Table II), compared to 70-min leaching at room temperature. Interestingly, the 24-h leaching in hot water did not remove all Na (~12% remained in insoluble phases), B (~22%), and Li (~54%) from the feed heated to 550°C.

IV. Discussion

(1) Feed Preparation ($T \leq 105$°C)

According to XRD and leaching test results, Na was present in the dry feed in the form of water-soluble salts, such as NaF, Na_2CrO_4, and Na_2SO_4, the fractions of which were too small to be detected by XRD, whereas NaOH likely reacted with H_3BO_3 in the slurry and formed sodium borates.[34,35] However, no crystalline borates were identified with XRD in feed samples and probably contributed to the amorphous (or, more precisely, unidentified crystalline) phase in the dry feed [Fig. 3(a)]. As Dolan and Misture[15] observed, borax dehydrated at ~130°C in a borosilicate batch, resulting in the formation of an amorphous phase.

Although most of the gibbsite remained stable during feed preparation [Fig. 3(a)], less than 1% of the Al leached from the dry feed [Table II and Fig. 4(c)], indicating that a small fraction of the gibbsite might form a soluble aluminate.

As XRD analysis of the dry feed shows [Fig. 3(b)], CaO turned to $CaCO_3$ in the slurry feed by reacting with Li_2CO_3 and $NiCO_3$ (as NiO formed $NiFe_2O_4$) and possibly with dissolved CO_2 in the slurry. Dehydration of $Fe(OH)_3$ to hematite began during drying, whereas trevorite had already formed during feed preparation.

(2) Dehydration of Feed (105°C $< T < 400$°C)

Previous works on thermogravimetric analysis (TGA),[28] and EGA[30] determined that the mass loss below 400°C was

Table II. Elements Dissolved from Heat-Treated Feeds (z_{ik}: Cumulative Fractions of Total)

Heat-treatment temperature, °C	105			350			550			
Leaching temperature, °C	Room *T*		80	Room *T*		80	Room *T*		80	
Leaching time, min	10	70	60	10	70	60	10	70	60	24 h
Na	0.9149	0.9418	0.9766	0.5639	0.7678	0.9176	0.2129	0.3869	0.5797	0.8826
B	0.8648	0.9026	0.9464	0.5383	0.7354	0.8726	0.1697	0.3106	0.4603	0.7851
Li	0.7730	0.8303	0.8764	0.4100	0.5016	0.6165	0.1263	0.1856	0.2333	0.4607
S	1	1	1	0.7197	0.8791	1	0.6132	0.7584	0.8543	NA
Al	0.0071	0.0067	0.0077	0.0036	0.0050	0.0143	0.0173	0.0255	0.0345	NA

NA, Not analyzed.

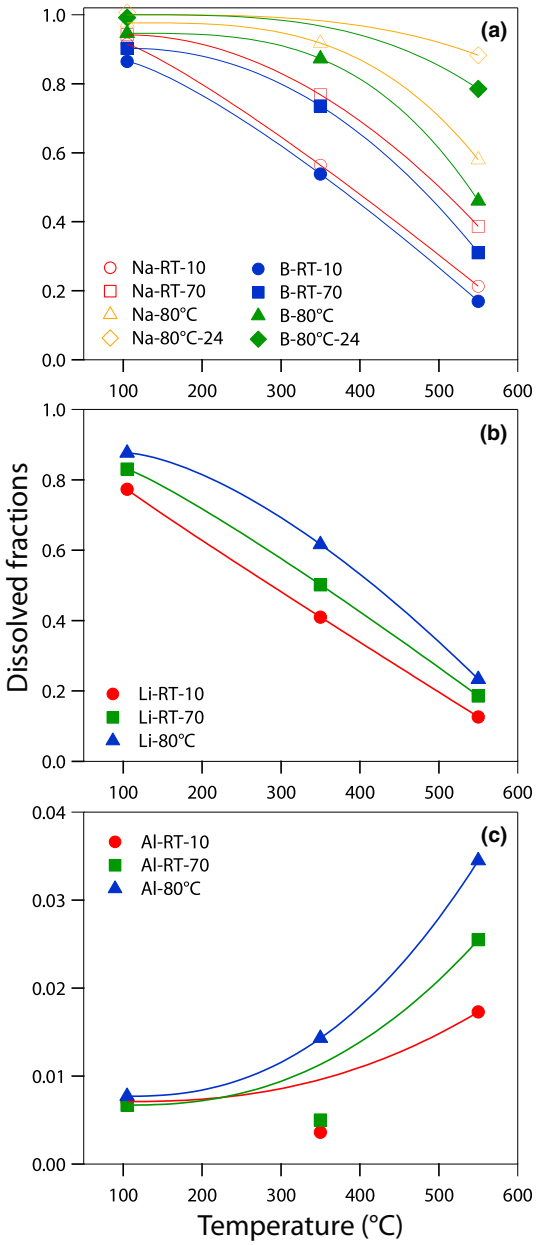

Fig. 4. Dissolved fractions of (a) Na and B, (b) Li, and (c) Al in different leaching steps as functions of heat-treatment temperature. RT = room temperature. Lines were added as guides to the eyes. Note that the dissolved fractions of Al from the 350°C sample by RT leaching are outliers.

mainly associated with H_2O release. Leaching tests, XRD, and SEM-EDS provide additional, though not yet complete, information about feed melting reactions.

As temperature increased, gibbsite lost water and disappeared before the temperature reached 400°C [Fig. 3(a)], partially turning to boehmite and mostly to amorphous Al_2O_3. The appearance of Al_2O_3 clusters, detected by SEM-EDS [Figs. 1(b) and (c)], dramatically increased the fraction of amorphous phase [Fig. 3(a)]. Borate phase that formed during feed preparation continued to lose water and formed a low-durability amorphous borate phase, as seen from room-temperature leaching data of the 350°C sample in Table II and Fig. 4(a).

$Fe(OH)_3$ dehydrated to hematite during drying, and continued dehydrating during heating, as evidenced by the slight increase in hematite content at $T \leq 400$°C [Fig. 3(b)]. Persistent agglomerates of hematite, Bi_2O_3, and ZrO_2, which were dehydrated from hydroxides, are seen in Figs. 1(b) and (c).

(3) Evolution of CO_2 and Formation of Early Glass-Forming Phase (400°C ≤ T ≤ 700°C)

Results of EGA[30] show that CO_2 evolution peaked at ~400°C, whereas $CaCO_3$ and Li_2CO_3 fractions continued to decrease and eventually vanished by 500°C [Fig. 3(b)]. Note that the discrepancy between CO_2 generation measured by EGA (as a function of temperature) and the carbonate decomposition as detected by XRD in crucible samples was caused by the effect of sample size on gas-evolving reactions.[21] The nascent CaO interacted with the amorphous phase, contributing to its decrease by forming $Ca_{0.5}NaAl_2B_2O_7$ above 500°C [Fig. 3(a)].

The ~20% Na leached from the sample heated to 550°C at room temperature (Table II) originated from water-soluble fluoride, chromate, sulfate, and borate. The leaching test results, Fig. 4(a), show that the early glass-forming phase became more durable as temperature increased, probably because of an increased content of Al_2O_3 and CaO. The smaller fraction of leached Li, compared to those of Na and B, suggests that less-soluble Li phases may have formed during heating, but those phases have not been identified yet.

In agreement with a study of quartz and spinel dissolution,[36] fine silica grains (≤75 μm) began to react with the early glass-forming melt above ~500°C, providing silica for the sodalite-nosean phase that was detectable with XRD, Fig. 3(b). Agglomerates of hematite, Bi_2O_3, and ZrO_2 persisted [Fig. 2(c)], whereas hematite started to convert to trevorite (or its solid solution with magnetite)[37] above 500°C.

(4) Implications for Cold-Cap Modeling and Nuclear Waste Vitrification

Cold-cap structure consists of two main regions, an open-porosity (reaction) layer from which batch gases escape through open pores to the atmosphere, and a foam layer, which comprises primary foam, cavities, and secondary foam.[9,10] The release of water, melting and decomposition of oxy-ionic salts and borates, and formation of intermediate crystalline phases, occur in the reaction layer. The main source of information about these reactions was thermal analyses.[28–30] This article provides additional information about the nature and fractions of the crystalline and amorphous phases involved. Their properties, such as heat

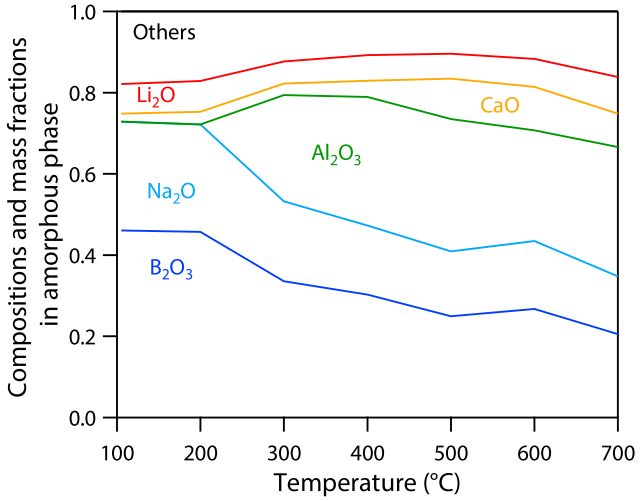

Fig. 5. Compositions and mass fractions in the amorphous phase versus heat-treatment temperatures.

capacities and reaction enthalpies, can be made readily available for cold-cap modeling.

The sensible heat and conversion heat for the feed reactions are transferred to the reaction layer from the melt pool. The foam layer that separates the reaction layer from the melt below acts as a heat insulator. Within the melt pool, the heat transfer is enhanced by vigorous convection produced by bubblers installed under the cold cap. Apart from bringing hot melt close to the cold cap, convective currents displace cavities and secondary foam,[5,38] thus further facilitating the heat flow. However, the primary foam layer remains and comes into direct contact with the hot melt, and continues to hinder heat transfer to the reaction layer.

Primary foam arises when enough glass-forming melt is produced within the melter feed that the viscous liquid becomes continuous, and evolving gases can no longer escape through open pores. Data presented in this work trace the development of the glass-forming phase. Hence, though restricted to the reaction layer, they are relevant to the foam development. The fraction of amorphous phase is presented in Fig. 3(a). Figure 5 shows its composition as assessed based on the chemical compositions of crystalline phases present. Over 75% of the amorphous phase consists of B_2O_3 and Na_2O in dry feed, the contribution of Al_2O_3 rose to ~30% at 300°C, and the CaO fraction increased above 400°C. Li_2O was present in the amorphous phase at a nearly constant level. Components such as Fe_2O_3, PbO, and Cr_2O_3 are included with the "Others". No SiO_2 was present in the glass-forming phase below 700°C.

However, the crystalline phases are rarely present in waste glasses as stoichiometric compounds. Considering this and the uncertainties of the crystalline fractions (Fig. 3), the evolution of the amorphous phase composition, shown in Fig. 5, indicates only a tendency rather than quantitative data. The portion of glass-forming melt in the amorphous material is unknown. For example, solid Al_2O_3, and CaO and some other amorphous metallic oxides, seen with SEM [Figs. 2(b) and (c)], only gradually dissolved in the borate melt as temperature increased. Therefore, we did not attempt to assess the viscosity of the glass-forming melt, even though we could assume that nearly all amorphous phase became glass-forming at 700°C, where, however, its composition lies outside the validity region of viscosity-composition models.[39] The emergence of the connected melt, the progressive dissolution of SiO_2, and the foaming above 700°C have been addressed in a previous paper.[40]

V. Conclusions

Batch reactions and phase transitions of a melter feed for vitrifying a high-alumina, high-level waste at $T \leq 700$°C were investigated by optical microscopy, scanning electron microscopy with energy-dispersive X-ray spectroscopy, X-ray diffraction, and leaching in cold and hot water. The feed was prepared in the form of slurry that was dried and then heated at 5 K/min. The main results can be summarized as follows.

1. In the slurry, CaO turned to $CaCO_3$, and NaOH likely reacted with H_3BO_3 to form sodium borates. Partial loss of water occurred during drying. For example, Fe $(OH)_3$ dehydrated to hematite.
2. At 105°C < T < 400°C, gibbsite dehydrated and disappeared by 400°C, turning mostly to amorphous Al_2O_3 and partially to boehmite, which existed up to 600°C. Sodium borates continued to lose water to form low-durability amorphous phases. The rest of the $Fe(OH)_3$ and other metallic hydroxides dehydrated to oxides.
3. At 400°C ≤ T ≤ 700°C, decomposition of $CaCO_3$ and Li_2CO_3 occurred before 500°C. Hematite converted to trevorite above 500°C. The sodium borate phase reacted with aluminum oxide and calcium oxide and formed the more durable amorphous phases along with intermediate crystalline products. Quartz started to dissolve into glass-forming melt.

Acknowledgments

This work was supported by the Department of Energy's Waste Treatment and Immobilization Plant Federal Project Office under the direction of Dr. Albert A. Kruger. The authors are grateful to Drs. Dong-Sang Kim, Jaehun Chun, and Tongan Jin for insightful discussions. Pacific Northwest National Laboratory is operated by Battelle Memorial Institute for the U.S. Department of Energy under contract DE-AC05-76RL01830.

References

[1]J. D. Vienna, "Nuclear Waste Vitrification in the United States: Recent Developments and Future Options," *Int. J. Appl. Glass Sci*, **1**, 309–21 (2010).
[2]K. S. Matlack, W. K. Kot, I. L. Pegg, and I. Joseph, *DM100 and DM1200 Melter Testing with High Waste Loading Glass Formulations for Hanford High-Aluminum HLW Streams*. Vitreous State Laboratory, VSL-09T1690-1, The Catholic University of America, Washington, DC, 2009.
[3]P. Hrma, A. A. Kruger, and R. Pokorny, "Nuclear Waste Vitrification Efficiency: Cold Cap Reactions," *J. Non-Cryst. Solids*, **358**, 3559–62 (2012).
[4]D. R. Dixon, M. J. Schweiger, B. J. Riley, R. Pokorny, and P. Hrma, "Temperature Distribution Within a Cold Cap During Nuclear Waste Vitrification," *Environ. Sci. Technol.*, (2015), doi: 10.1021/acs.est.5b00931.
[5]R. Pokorny, et al., "Cold Cap Model for Melters with Bubblers," *J. Am. Ceram. Soc.* (in press).
[6]M. J. Plodinec, "Vitrification Chemistry and Nuclear Waste," *J. Non-Cryst. Solids*, **84**, 206–14 (1986).
[7]G. Roth and S. Weisenburger, "Vitrification of High-Level Liquid Waste: Glass Chemistry, Process Chemistry and Process Technology," *Nucl. Eng. Des.*, **202**, 197–207 (2000).
[8]R. E. Eibling and C. A. Nash, *Hanford Waste Simulants Created to Support the Research and Development on the River Protection Project-Waste Treatment Plant*. Westinghouse Savannah River Company, WSRC-TR-2000-00338, Aiken, SC, 2001.
[9]R. Pokorny and P. Hrma, "Mathematical Modeling of Cold Cap," *J. Nucl. Mater.*, **429**, 245–56 (2012).
[10]R. Pokorny and P. Hrma, "Model for the Conversion of Nuclear Waste Melter Feed to Glass," *J. Nucl. Mater.*, **445**, 190–9 (2014).
[11]H. Verweij, H. van den Boom, and R. E. Breemer, "Raman Spectroscopic Study of the Reactions in a Potassium Carbonate-Silicate Glass-Forming Batch," *J. Am. Ceram. Soc.*, **61**, 118–21 (1978).
[12]K. S. Hong and R. E. Speyer, "Thermal Analysis of Reactions in Soda-Lime Silicate Glass Batches Containing Melting Accelerants: I, One- and Two-Component Systems," *J. Am. Ceram. Soc.*, **76**, 598–604 (1993).
[13]K. S. Hong and R. E. Speyer, "Thermal Analysis of Reactions in Soda-Lime Silicate Glass Batches Containing Melting Accelerants: II, Multicomponent Systems," *J. Am. Ceram. Soc.*, **76**, 605–8 (1993).
[14]D. S. Kim and J. Matyáš, *Batch Reactions of a Soda-Lime Silicate Glass*. Pacific Northwest National Laboratory, PNNL-13994, Richland, WA, 2002.
[15]A. R. Jones, R. Winter, G. N. Greaves, and I. H. Smith, "^{23}Na, ^{29}Si, and ^{13}C MAS NMR Investigation of Glass-Forming Reactions Between Na_2CO_3 and SiO_2," *J. Phys. Chem. B*, **109**, 23154–61 (2005).
[16]F. Raether and M. Krauβ, "In Situ Measurement of Batch Glass During Melting," *Glass Sci. Technol.*, **77**, 118–23 (2004).

[17]M. D. Dolan and S. T. Misture, "Analysis of Glass Batch Reactions Using *in Situ* X-Ray Diffraction. Part I. Batch Components and Binary Quartz Mixtures," *Glass Technol.*, **45**, 140–7 (2004).
[18]M. D. Dolan and S. T. Misture, "Analysis of Glass Batch Reactions Using *in Situ* X-Ray Diffraction. Part 2. Soda-Lime-Silica Glass Batches," *Glass Technol.*, **45**, 167–74 (2004).
[19]M. D. Dolan and S. T. Misture, "Analysis of Glass Batch Reactions Using *in Situ* X-Ray Diffraction. Part III. Borosilicate Glass Batches," *Glass Technol.*, **45**, 212–9 (2004).
[20]E. Gouillart, et al., "In Situ Synchrotron Microtomography Reveals Multiple Reaction Pathways During Soda-Lime Glass Synthesis," *J. Am. Ceram. Soc.*, **95**, 1504–7 (2012).
[21]P. Hrma, "Batch Melting Reactions"; Chapter 5, pp. 157–76 in *Chemistry of Glass*, Edited by A. Paul. Chapman and Hall, London, New York, 1990.
[22]P. Hrma, J. Marcial, K. J. Swearingen, S. H. Henager, M. J. Schweiger, and N. E. TeGrotenhuis, "Conversion of Batch to Molten Glass, II: Dissolution of Quartz Particles," *J. Non-Cryst. Solids*, **357**, 820–8 (2011).
[23]P. Hrma, et al., "Effect of Glass-Batch Makeup on the Melting Process," *Ceram. Silikáty*, **54**, 193–211 (2010).
[24]S. H. Henager, P. Hrma, K. J. Swearingen, M. J. Schweiger, J. Marcial, and N. E. TeGrotenhuis, "Conversion of Batch to Molten Glass, I: Volume Expansion," *J. Non-Cryst. Solids*, **357**, 829–35 (2011).
[25]D. A. Pierce, P. Hrma, J. Marcial, B. J. Riley, and M. J. Schweiger, "Effect of Alumina Source on the Rate of Melting Demonstrated with Nuclear Waste Glass Batch," *Int. J. Appl. Glass Sci.*, **3**, 59–68 (2012).
[26]K. Watanabe, T. Yano, K. Takeshita, K. Minami, and E. Ochi, "X-Ray CT Image of Vitrified Glasses Containing Simulant Radioactive Wastes: Structure and Chemical Reactions of Glass Beads and Wastes in the Cold Cap," *Glass Technol.: Eur. J. Glass Sci. Technol. A*, **53**, 273–8 (2012).
[27]Y. Okamoto, et al., "High-Temperature X-Ray Imaging Study of Simulated High-Level Waste Glass Melt," *Electrochemistry*, **81**, 543–6 (2013).
[28]R. Pokorny and P. Hrma, "Melting of Glass Batch: Model for Multiple Overlapping Gas-Evolving Reactions," *Thermochim. Acta*, **541**, 8–14 (2012).
[29]J. Chun, D. A. Pierce, R. Pokorny, and P. Hrma, "Cold-Cap Reactions in Vitrification of Nuclear Wastes Glass: Experiments and Modeling," *Thermochim. Acta*, **559**, 32–9 (2013).
[30]C. Rodriguez, J. Chun, M. J. Schweiger, A. A. Kruger, and P. Hrma, "Application of Evolved Gas Analysis to Cold-Cap Reactions of Melter Feeds for Nuclear Waste Vitrification," *Thermochim. Acta*, **592**, 86–92 (2014).
[31]K. Xu, D. A. Pierce, P. Hrma, M. J. Schweiger, and A. A. Kruger, "Rhenium Volatilization in Waste Glasses," *J. Nucl. Mater.*, **464**, 382–8 (2015).
[32]K. S. Matlack, et al., *Melt Rate Enhancement for High Aluminum HLW Glass Formulations*. Vitreous State Laboratory, VSL-08R1360-1, The Catholic University of America, Washington, DC, 2008.
[33]M. J. Schweiger, P. Hrma, C. J. Humrickhouse, J. Marcial, B. J. Riley, and N. E. TeGrotenhuis, "Cluster Formation of Silica Particles in Glass Batches During Melting," *J. Non-Cryst. Solids*, **356**, 1359–67 (2010).
[34]E. M. Levin, C. R. Robbins, and H. F. McMurdie, *Phase Diagrams for Ceramists Vol. I*, pp. 534. The American Ceramic Society, Columbus, Ohio, 1964.
[35]E. M. Levin and H. F. McMurdie, *Phase Diagrams for Ceramists Vol. III*, pp. 432. The American Ceramic Society, Westerville, Ohio, 1975.
[36]R. Pokorny, J. A. Rice, J. V. Crum, M. J. Schweiger, and P. Hrma, "Kinetic Model for Quartz and Spinel Dissolution During Melting of High-Level-Waste Glass Batch," *J. Nucl. Mater.*, **443**, 230–5 (2013).
[37]J. Alton, T. J. Plaisted, and P. Hrma, "Dissolution and Growth of Spinel Crystals in a Borosilicate Glass," *J. Non-Cryst. Solids*, **311**, 24–35 (2002).
[38]R. Pokorny, A. A. Kruger, and P. Hrma, "Mathematical Modeling of Cold Cap: Effect of Bubbling on Melting Rate," *Ceram. Silikáty*, **58**, 296–302 (2014).
[39]P. Hrma and S. S. Han, "Effect of Glass Composition on Activation Energy of Viscosity in Glass-Melting-Temperature Range," *J. Non-Cryst. Solids*, **358**, 1818–29 (2012).
[40]J. Marcial, J. Chun, P. Hrma, and M. J. Schweiger, "Effect of Bubbles and Silica Dissolution on Melter Feed Rheology During Conversion to Glass," *Environ. Sci. Technol.*, **48**, 12173–80 (2014). □